LANGMUIR

Interface Components: Nanoparticles, Colloids, Emulsions, Surfactants, Proteins, Polymers

Ionic environment affects bacterial lipopolysaccharide packing and function

Ali Rahnamoun, Kyoungtea Kim, Joel A. Pedersen, and Rigoberto Hernandez

Langmuir, **Just Accepted Manuscript** • DOI: 10.1021/acs.langmuir.9b03162 • Publication Date (Web): 18 Feb 2020

Ionic environment affects bacterial lipopolysaccharide packing and function

Ali Rahnamoun[†], *Kyoungtea Kim*[‡], *Joel A. Pedersen*[‡,§], *and Rigoberto Hernandez*[*†]

[†] Department of Chemistry, Johns Hopkins University, Baltimore, Maryland 21218, United States

[‡] Molecular and Environmental Toxicology Center, University of Wisconsin-Madison, Madison, Wisconsin 53706, United States

[§] Departments of Soil Science, Chemistry, Civil & Environmental Engineering, University of Wisconsin-Madison, Madison, Wisconsin 53706, United States

Abstract. The interaction of lipopolysaccharides (LPS) with metal cations strongly affects the stability and function of the Gram-negative bacterial outer membrane. The sensitivity of deep rough (Re) LPS packing and function to the ionic environment, as affected by cation valency and ionic radius, has been determined using molecular dynamics simulations and Langmuir balance experiments. The degree of LPS aggregation within the LPS models in the presence of different cations is assessed by measuring the effective mean molecular area ($\hat{A}_m$) of each LPS molecule projected onto the interfacial plane at the end of the equilibration. These results are compared to the LPS mean molecular area from experimental measurements in which the LPS monolayers are assembled at the air-water interface using a Langmuir film balance. We found that packing of the LPS arrays is sensitive to the ionic radius and ion valency of the cations present in solution during LPS array packing. Using enhanced sampling of the free energy for the intercalation of oligo(allylamine HCl) (OAH) into deep rough *Salmonella enterica* LPS bilayers, we obtained the affinity of the core section of LPS to OAH as a function of the nature of the metal cations present in solution. We found that packing of the solvated LPS bilayer models is sensitive to ionic radius and ion valency of the neutralizing cations. This further suggests that ion bridging and steric barriers rather than charge shielding are important factors in mitigating ligand intercalation under conditions with low ionic concentrations.

1. Introduction

Our ability to determine chemical responses of the outer membrane of bacteria is limited by the small size of bacteria and the complexity of its structure. For Gram-negative bacteria, that structure primarily consists of lipopolysaccharide (LPS) molecules with a typical coverage of 75%

of the surface[4], and acts as the first line of resistance for bacteria against adverse environments. The molecular structure of full-length LPS molecules is typically characterized by three distinct regions: (1) the innermost hydrophobic lipid component called lipid A being anchored in the bacterial outer membrane; (2) the core oligosaccharide linked with lipid A; and (3) the *O*-polysaccharide polysaccharide linked with the core oligosaccharide. LPS molecules that include all three domains are called smooth, while LPS lacking the *O*-polysaccharide are called rough. In this work, we focused on the LPS molecule of *Salmonella enterica* Re 595 (deep rough) mutant as shown schematically at the bacterial interface in Fig. 1A, and in near atomic resolution in Fig. 1B. LPS molecules have high levels of structural diversity because of the different combinations of lipid A, core oligosaccharides and *O*-polysaccharide regions. With advances in experimental measurements[5] and simulations[6] of such complex model structures along with increasing computational resources, uncovering their structural properties and dynamics is becoming increasingly accessible, making it possible to better interrogate the role of LPS within the outer layer of Gram-negative bacteria at the molecular scale.

The improved characterization and prediction of variations in the LPS structures, packing, rigidity, and permeability on the outer membrane of Gram-negative bacteria has emerged as critical to designing both antibacterial and benign materials.[7-18] The interactions between nanoparticles and bacterial surface LPS are governed by nanoparticle surface coating.[19] The hydrophilic region formed by sugar residues in the core oligosaccharide and *O*-polysaccharide sections of LPS molecules on the outer surface of bacteria acts as a barrier against penetration of hydrophobic antibacterial molecules.[20] Investigating the role of cations residing between the LPS molecules on the LPS conformation is a key to understanding the resistance to penetration of hydrophobic antibacterial molecules. In this work, we have characterized the effect of monovalent and divalent cations on the intermolecular density (or loading) so as quantify this effect. Previous studies found that gold nanoparticles (AuNPs) with positively charged coatings are often significantly more toxic than AuNPs functionalized with anionic coatings.[21-22] In particular, functionalization with cationic poly(allylamine hydrochloride) (PAH) polymers has led to substantially higher lethality to bacteria and water flea *Daphina magna* than negatively charged particles.[19, 21] Unfortunately, the typical long lengths of PAH make the entire system too large to model with existing computational resources. Instead, we expose the LPS to the shorter oligo (allylamine hydrochloride) (OAH). This allows us to interrogate the direct chemical interaction between the coating of a functionalized AuNPs and LPS in the presence of different cations with the caveat that we do not account for possible entropic interactions from the longer chains.

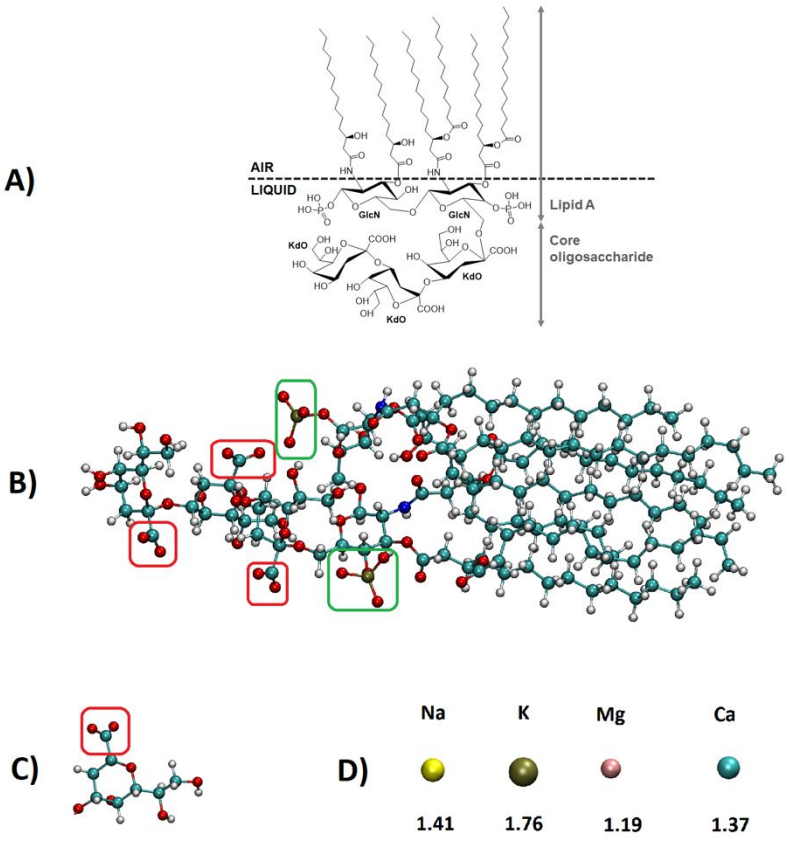

Figure 1. The structure of the molecules of interest to this work: (A) Schematic representation of *Salmonella enterica* deep rough LPS molecule at the air-water interface, highlighting the presence of D-glucosamine (GlcN) and 3-deoxy-d-*manno*-octulosonic acid (Kdo) ad various positions within the liquid region. (B) deep rough LPS of *Salmonella enterica* with the carboxyl group from the Kdo sugars and the phosphoryl groups highlighted with red and green squares, respectively, (C) the Kdo sugar with the carboxyl group corresponding to those in structure A also highlighted by a red box, and (D) cations shown by spheres with the radii[1] (in Ångströms) from the CHARMM parameter set.[2-3] Assuming complete deprotonation, the total charge of the Lipid A section is -4 and the total charge of the core section is -3, introducing the total charge of -7 for the LPS molecules. Carbon atoms are shown in cyan color, Oxygen atoms are shown in red color, Hydrogen atoms are shown in White color and Phosphorous atoms are shown in dark gold color.

Prior experimental studies of bacterial LPS have partially resolved the effects of the ionic environment on LPS conformations and function. Schneck et al.[23] reconstructed electron density profiles from X-ray reflectivity curves and concluded that the presence of Ca^{2+} ions induces a considerable change in the conformation of the charged polysaccharide head groups of LPS of *Pseudomonas aeruginosa*. Their results indicated that the *O*-polysaccharide chains collapse towards the LPS core oligosaccharide region in the presence of Ca^{2+} ions which can increase bacterial resistance to cationic antimicrobial peptides. Le Brun et al.[24] created stable monolayers

of pure *Escherichia coli* RcLPS (lipid A plus the first seven sugar residues of the core oligosaccharide) at the air−liquid interface. They showed that Langmuir monolayers are able to produce model monolayer surfaces with realistic surface topology and molecular fluidity. Garidel et al.[25] measured the structural parameters of deep rough lipopolysaccharide (ReLPS) from *Salmonella enterica* in the presence of Mg^{2+}, Ca^{2+}, and Ba^{2+} using synchrotron radiation X-ray diffraction. They showed that the unilamellar/cubic inverted aggregate LPS structures are converted into multilamellar structures by divalent alkali earth metal cations independent of ion identity. Clifton et al.[26] employed X-ray reflectivity and neutron reflectivity to determine the effects of divalent cations on the structural integrity of rough strains of LPS molecules from *E. coli*. They found that, without the charge screening effects of divalent cations, the rough LPS molecules flip across the hydrophobic bilayer resulting in some degree of mixing between LPS and a phospholipid originally from the inner leaflet. Schneck et al.[27] measured the density profiles of monovalent K^+ and divalent Ca^{2+} cations normal to *S. enterica* rough mutant LPS monolayers using grazing incidence X-ray fluorescence. They reported that divalent cations displace monovalent cations from the headgroup region. Kučerka et al.[28] determined the penetration of water molecules through *Pseudomonas aeruginosa* PAO1 LPS bilayers from the difference between one-dimensional neutron scattering length density (1D SLD) profiles. They found that Ca^{2+}-loaded LPS bilayers experience reduced water penetration compared to Mg^{2+}- or Na^+-loaded LPS bilayers. Recently, Micciulla et al.[29] characterized the monolayer strucrture in wild-type LPS from *Escherichia coli* O55:B5 at the air-water interface by combined x-ray reflectometry (XRR) and neutron reflectometry (NR). While XRR offers good contrast between the air and fatty acid chains, NR has the advantage that it can distinguish between water and hydrated saccharides. Similar to many previous studies, they observed ion-specific bridging with the LPS anionic groups for LPS monolayers loaded with Ca^{2+} divalent cations which goes beyond generic electrostatic interactions. Before this, Rodriguez-Loureiro et al.[30] performed NR measurements on similar LPS types and found saccharide profiles to be bimodal, with dense inner oligosaccharides and more dilute, extended *O*-side chains.

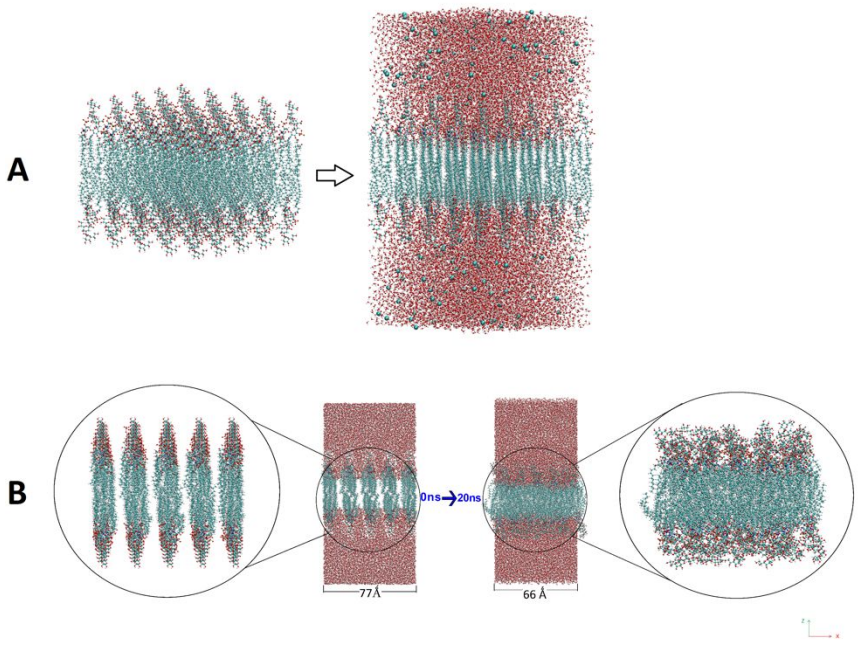

Figure 2. (A) Deep rough *Salmonella enterica* LPS bilayer solvated in explicit water molecules and charge neutralized with Ca^{2+} cations. Each leaflet of the LPS bilayer contains 25 LPS molecules. (B) LPS bilayer NPT equilibrations at atmospheric pressure with flexible periodic boundary conditions in *X*, *Y* and *Z* directions. The *X* and *Z* axes are as indicated, and the *y*-axis is perpendicular to the *XZ* plane.

Meanwhile, recent advances in the parameterization of LPS molecules and increasing computational power have opened the possibility of modeling these complex systems from atomic resolution to larger scales. Ma et al.[31] developed a parameter set for LPS in a coarse-grained representation using the standard bead types of the MARTINI force field to calculate structural and thermodynamic properties of LPS models with different compositions. Wu et al.[32] simulated several all-atom bilayers with varying core and *O*-polysaccharide repeating units and showed that increasing the LPS molecular length impacts LPS structure and dynamics. They further observed that lateral per-lipid area increases and lipid bilayer order decreases as the core and *O*-antigen are successively included in the representations. Lam et al.[33] developed a coarse-grained model to describe electrostatic modifications to the LPS layer by Mg^{2+}, ethylene-diaminetetraacetic acid (EDTA), and antimicrobial peptides (AMPs). Their results show that Mg^{2+} tightens the LPS layer while EDTA or AMPs counteract the lateral packing by displacing previously bound Mg^{2+} ions from the LPS layer. Pink et al.[34] performed both experiments and simulations to confirm that addition of Ca^{2+} significantly reduces the binding of protamine, a cationic antimicrobial peptide, to LPS from *Ps. aeruginosa* PA01 and *E. coli* and consequently reduces its antimicrobial activity. They showed that the protamine distribution, in the presence of divalent cations, depends on monovalent ion concentration, and that in the absence of divalent cations, protamine distribution is independent of monovalent cation concentration. Kim et al.[35]modeled homogeneous lipid bilayers of 21 distinct lipid A types from 12 bacterial species using all-atom molecular dynamics (MD) simulations and showed the influence of neutralizing ions on the stability and the integrity of

lipid A bilayers have been reported to be minimal. Piggot et al.[36] characterized the dynamic properties of the bacterial outer membrane of *E. coli* using all-atom MD simulations, evaluating the mobility of the lipids within the monolayers and observed slower diffusion for lipid A relative to phospholipids. Furthermore, MD simulations using GLYCAM[37], OPLS[38], AMBER[39] and GROMOS[36] force fields have earlier been performed to reveal structural, dynamical and electrostatic properties of bacterial LPS. The challenge, addressed here, is the determination of the effect of varying ion concentration and identity on LPS packing. This multiscale phenomenon has been resolved through a combination of simulation and experiment.

In this work, we have implemented atomistic MD simulations to quantify the effect of divalent (Ca^{2+}, Mg^{2+}) and monovalent (Na^{+}, K^{+}) cations (Fig.1) on the LPS bilayer structure at atomic resolution. As indicated in Fig. 1, the ionizable groups in the LPS molecules are all assumed to be fully deprotonated following some reports (discussed above) of complete dehydrogenation in the presence of the cations, and allowing a reduction in the number of configurations that must be modeled. We note that this is a strong assumption, and that the charge of -7 on the LPS molecule listed in Fig. 1 must be considered an upper limit because of partial protonation. We used the CHARMM36 lipid and carbohydrate force field,[2] and propagated trajectories with the NAMD integrator.[40] This force field is compatible with the additive all-atom parameters required for proteins, nucleic acids, carbohydrates and general organic molecules in this work. The results of the MD simulations were compared to experimentally determined LPS mean molecular areas obtained from interfacial monolayers using a Langmuir film balance. We find that the resulting LPS aggregation varies markedly with respect to cation charge, and ionic radius. The simulations provide a molecular view of the contraction of the LPS layer by revealing the effect of ionic parameters and LPS functional groups.

2. Methods

2.1. LPS packing simulations

The structure of deep rough LPS (Re mutant) of *Salmonella enterica* is shown in Fig.1. Each deep rough ReLPS molecule includes three Kdo sugar residues and two phosphoryl groups. Each Kdo residue includes one carboxyl group. *O*-Polysaccharides are entirely absent in rough LPS. Additional details about the number of phosphoryl groups and total charge of these LPS models are listed in SI Table S1.

We simulated model bilayers composed of 25 deep rough ReLPS 595 of *S. enterica* in rectilinear configurations in each leaflet (Fig. 2A) and imposed periodic boundary conditions. The LPS bilayers were solvated with explicit water molecules and neutralized with the chosen cations. To prevent unrealistic hydrophobic effects in our simulation arising from the limitations of the periodic boundary conditions, we removed the water molecules from the hydrophobic section at the edges of the bilayers. The charge of the solvated LPS models was neutralized using the minimum number of cations, and the appropriate chloride salt was added to attain concentrations of 1.5 mM for systems loaded with divalent cations (Ca^{2+}, Mg^{2+}) and 3mM for systems loaded with monovalent cations (Na^{+}, K^{+}). Ionic radii are given in Fig. 1D in Ångströms.[1]

After building the LPS bilayer, solvating and neutralizing with Ca^{2+}, Mg^{2+}, Na^{+}, or K^{+} cations in separate systems and adding the corresponding extra chloride salts, the simulations were performed in the following steps: (1) with the core section, water molecules and ions fixed, the systems were equilibrated allowing the lipid A molecules to move and melt; (2) with the core section fixed, water molecules and ions were released and allowed to equilibrate at T=294 K; and(3) all the restraints on the system were removed and NPT equilibration (constant number of atoms, pressure and temperature) was performed with flexible periodic boundary conditions in all directions. After removing the equilibration restraints from solvated and ionized LPS bilayer models, they started to shrink in the *XY* plane, requiring the walls to move in so as to maintain the pressure. Initial and final snapshots of a 20ns equilibration simulation are shown in Fig. 2B. To evaluate the packing of LPS molecules in the bilayer models at the end of equilibrations, we measured the effective mean molecular area per LPS molecules in the *XY* plane of the models ($\hat{A}_m$). This parameter is used as a general metric of packing in the membrane plane. These measurements are performed at the end of equilibrations while the $\hat{A}_m$ of the model in the membrane plane fluctuates around a steady average value. All the solvated and ionized LPS bilayers are equilibrated for at least 20 ns using a 2 fs simulation time step. The curves for $\hat{A}_m$ in these systems all decay from the perturbed initial condition to equilibrium well within 20 ns of simulation time (cf. Fig. S1 in SI), confirming this choice for the maximum integration time in the simulated trajectories.

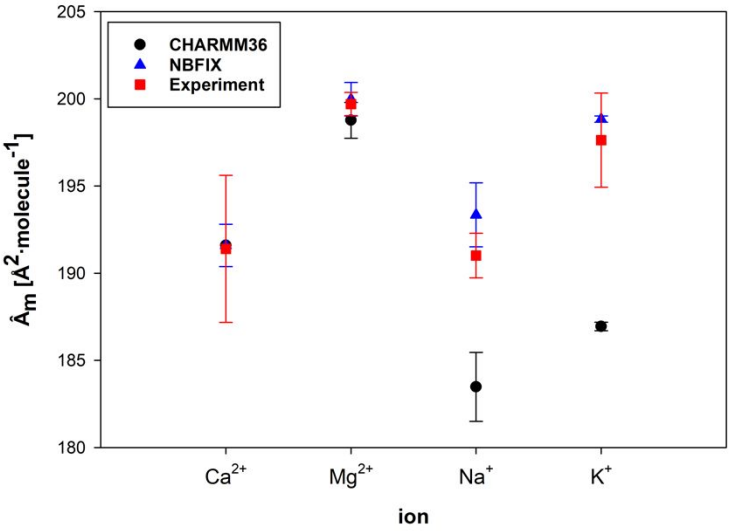

Figure 3. Mean molecular area ($\hat{A}_m$) for *Salmonella enterica* deep rough LPS molecules in bilayer models. The reported values and error bars are calculated by taking averages over the last 1 ns frames of two *NPT* equilibration trajectories for each solvated LPS bilayer loaded with the indicated cation(s) for two cases: (1) Standard, in which the standard CHARMM parameters are employed in the simulations, and (2) NBFIX in which the NBFIX correction is applied. Experimental results are means and standard deviations of $\hat{A}_m$ obtained at a compression modulus of 20 mN·m^{-1} from quadruplicate Π–$\hat{A}_m$ isotherms. Representative isotherms are displayed in Fig. 6.

2.2. Free energy calculations of ligand binding affinity to the LPS arrays

An LPS array in the presence of each of the cations selected for this work was first equilibrated. Each of these LPS arrays was exposed to a10-mer oligo allylamine HCl(OAH)used as a surrogate for poly(allylamine HCl). The OAH was placed on top of a given solvated LPS array with minimum distance of 50Å between the center of mass (COM) of OAH and the COM of the carbon atoms of the acyl chain terminal methyl group of the lipid A sections of the LPS molecules. To probe the interactions of OAH with an equilibrated LPS model, free energy calculations utilizing adaptive biasing force (ABF) are performed.[41] We measure computational free energy changes for the motion of an OAH from above an LPS model towards the middle of the LPS bilayer. Using the ABF method, the free energy changes are calculated while the *Z* direction distance, normal to the membrane plane between the COM of OAH and the COM of the carbon atoms of the acyl chain terminal methyl group of the lipid A sections of the LPS molecules are varied between 50-10 Å (cf. Fig. S2 in SI). To achieve more accurate results and increase the sampling at different locations, the ABF free energy calculations are performed in 10 Å interval windows. Each window is defined by a minimum and maximum *Z* direction distance between the COMs.

2.3. Materials

We purchased Re 595 LPS from *S. enterica* serotype Minnesota, sodium chloride (>99.999%), magnesium dichloride (≥99.99%), and chloroform (≥99.8%) from MilliporeSigma (Burlington, MA, USA). The LPS was used without further purification. Calcium dichloride (≥99.9965%) and

potassium chloride (≥99.999%) were procured from Thermo Fisher Scientific (Waltham, MA, USA), and methanol (>99.9 %) was obtained from Honeywell (Morris Plains, NJ, USA). Ultrapure water (resistivity 18.2 MΩ·cm) was produced by GenPure Pro UV-TOC/UF (Thermo Fisher Scientific, Waltham, MA, USA). To minimize ion contamination from labware we carefully cleaned all glassware, the Langmuir-Blodgett trough, and the movable barriers with Tween 20 (MilliporeSigma, Burlington, MA, USA) followed by more than five rinses with deionized water and more than five rinses with ultrapure water. The Langmuir-Blodgett trough and the barriers were further rinsed with ethanol and ultrapure water per manufacturer recommendations.

2.4. Formation of Langmuir monolayers

To assess the impact of ions on LPS monolayers at the air-liquid interface, we constructed surface pressure (Π)–mean molecular (surface) area ($\hat{A}_m$) isotherms measuring Π by the Wilhelmy plate method using a platinum plate.[42] Salts and salt solutions were pretreated to minimize effects of by organic contamination.[43] Salts of monovalent cations were baked at 650 °C for 10 h, and divalent salt solutions were filtered three times through an activated carbon filter (Whatman Carbon Cap 75, Thermo Fisher Scientific, Waltham, MA, USA).

We dissolved Re 595 LPS in chloroform and methanol (9:1 v/v) mixture at a concentration of 0.5 g·L^{-1}. An interfacial monolayer was formed by allowing a 60 µL aliquot of Re LPS solution to spread at the air-liquid interface in a KN2002 Langmuir-Blodgett trough (KSV NIMA, Gothenburg, Sweden) filled with 190 mL of water or salt solutions. After depositing the Re LPS solution, we allowed the chloroform and methanol to evaporate from the interface for 30 min. After the monolayer had equilibrated as evidenced by a stable initial surface pressure (Π_0), the interface was compressed by two barriers at a speed of 5 Å^2·molecule^{-1}·min^{-1}. As remarked in the introduction, Figure 1A shows a possible arrangement of an LPS molecule at the air-liquid interface in which the hydrophobic acyl chains extend away from the liquid surface. All measurements were performed at a temperature of 21 °C (294 K) that was maintained by an F12-MA refrigerated/heating circulator (Julabo, Seelbach, Germany). Monolayer area compression moduli, K_A, were obtained from slopes of the Π–$\hat{A}_m$ isotherms as [44]

$$K_A = -\hat{A}_m \left(\frac{\partial \Pi}{\partial \hat{A}_m} \right)_T \qquad (1)$$

where Π and $\hat{A}_m$ are defined as above, and T is temperature. First derivatives of each isotherm were determined using Prism 8.0.1 (GraphPad, San Diego, CA, USA) with the second-order smoothing polynomial option. Molecular configurations of interfacial monolayers are defined by the magnitude of K_A; the bidimensional gaseous (G), liquid expanded (LE), liquid condensed (LC), and solid states correspond respectively to values of K_A <10 mN·m^{-1}, 10 – 50 mN·m^{-1}, 100 – 250 mN·m^{-1}, and 1000 – 2000 mN·m^{-1}.[44] In the present work, we selected a value of K_A = 20 mN·m^{-1} to correspond to the LE state near the transition between G and LE states as a metric to compare the impacts of cations on LPS monolayer packing. The G-to-LE transition corresponds to the point

in the Π–$\hat{A}_m$ isotherms representing the initiation of molecule-molecule interactions at the air-water interface.[45]

2.5. Inductively coupled plasma-mass spectrometry

Calcium and magnesium from labware[46] or associated with LPS[47] can in principle affect the measured mean molecular areas. We thoroughly cleaned all labware (*vide supra*). To define the Ca^{2+} and Mg^{2+} concentrations under the experimental conditions, we measured these elements in our solutions by inductively coupled plasma mass spectrometry (ICP-MS) using an Element2 SF-ICP-MS (ThermoFisher Scientific, Waltham, MA, USA) with a PFA nebulizer and quartz spray chamber. The spectrometer was equipped with ESI SC-2 DX autosampler (Elemental Scientific, Omaha, NE, USA) with PC FAST switching valve and 2.5 mL loop. Ion concentrations were determined by a method described previously.[48] Solutions of LPS and salts were diluted 1/2 and 1/20 with 2% HNO_3 for the analyses, respectively. Experimental parameters are presented in Table S2 in the SI.

3. Results

3.1. LPS packing in different ionic environments

For each LPS bilayer model solvated and charge neutralized by Ca^{2+}, Mg^{2+}, Na^+ or K^+ cations and with the corresponding extra salts added, two equilibration trajectories were generated and $\hat{A}_m$ values for each of these systems were calculated during the final 1 ns when the systems were well-equilibrated. The standard CHARMM36 lipid and carbohydrate force fields were employed in these simulations. The calculations of the $\hat{A}_m$ values for the systems loaded with varying cations from simulation were compared to the values obtained from Langmuir film balance experiments. Figure 3 reports the values of $\hat{A}_m$ for the *Salmonella enterica* deep rough LPS molecules observed in these simulations performed using the standard CHARMM force field (reported in this section) and in experiments (reported below in Sec. 3.3). For the systems loaded with divalent cations, these values show good agreement between the simulations and experimental measurements reported here and previously.[49] For systems loaded with monovalent cations, simulations using the standard CHARMM parameters overestimated the binding of cations to the LPS molecules. This leads to artificial aggregation of the LPS arrays loaded with these monovalent cations. This suggests that the standard force field parameters may not be appropriate for the characterizing highly charged molecules like LPS even if they work well for less charged or neutral cases.

As an alternative, the improved CHARMM force field with tuned non-bonded interaction parameters (NBFIX) was utilized for the packing simulations of LPS arrays loaded with monovalent cations. Improvements to the force field by NBFIX includes the refinement of the LJ radii (R_{min}), in which the atom pair-specific adjustments to the non-bonded interactions are calibrated against experimentally measured quantities for proteins, nucleic acids, and lipids.[50-51] Pair-specific non-bonded interactions between Na^+ and K^+ cations and oxygen atoms of carboxyl and phosphoryl groups (as illustrated in the inset of Fig. S3 in the SI) were implemented to decrease the binding estimation of these cations to the charged molecules. The original CHARMM LJ radii for the interactions between monovalent cations and oxygen atoms of carboxyl and

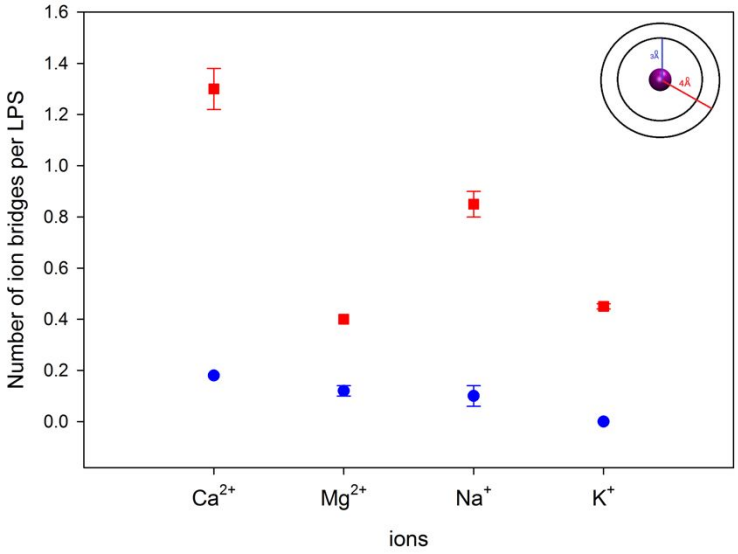

Figure 4. Number of bridges that ions make between carboxyl-carboxyl, carboxyl-phosphoryl or phosphoryl-phosphoryl groups within radial distances of 3 Å (blue filled circles) and 4 Å (red squares).

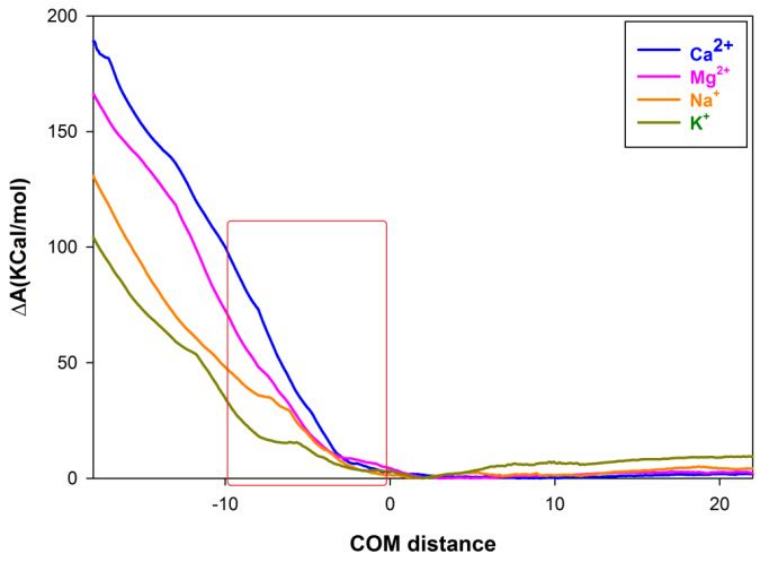

Figure 5. Helmholtz free energy differences (Δ*A*) for the interaction of oligo(allylamine HCl) to the deep rough *Salmonella enterica* LPS bilayer at distances far from the bilayer (22 Å) to the LPSbilayer surface (0 Å) and to deep intercalation at –18 Å. It is obtained using ABF free energy calculation as described in the text. The range highlighted by the rectangle shows the locations that the LPS anionic groups are concentrated.

phosphoryl groups and the corresponding tuned values —representing a little less than a 5% increase— are illustrated in Fig. S3 of the SI.

The packing results for all the four cations using the augmented force field are shown in Fig. 3. Utilizing the NBFIX feature of CHARMM force field lead to $\hat{A}_m$ values which were in good agreement with the corresponding experimental results for Ca^{2+}-, Mg^{2+}-, Na^{+}-,andK^{+}-loaded LPS arrays. Increasing in the Lennard-Jones R_{min} by maximum3% is sufficient to reduce monovalent cation binding to oxygen atoms of carboxyl and phosphoryl groups, and thereby increase surface areas per LPS by around 6% compared with the unmodified parameters.

The trends observed in Fig. 3 indicate that $\hat{A}_m$, which represents the degree of packing of the LPS array, depends on the ionic parameters (ionic radius, valency). This suggests a combination of ionic radius and valency parameters can determine the degree of LPS packing. When the system is loaded with divalent cations, the cations were seen to bridge between anionic groups in various configurations such as those shown in Fig. S4 of the SI. We thus find that larger diameter cations (e.g., Ca^{2+}) lead to more packing in an LPS bilayer than smaller diameter cations (e.g., Mg^{2+}).This trend in packing is also consistent with reports[52] that the hydration radius of Ca^{2+} (4.12 **Å**) is smaller than that of Mg^{2+} (4.28 **Å**) which we did not explicitly determine in our simulations because they are well known. It is also consistent with the fact that the waters of hydration are held more tightly for Mg^{2+} (mean residence time for H_2O in the primary hydration sphere, τ = ~1.5 × 10^{-6} s) than for Ca^{2+} (τ = ~10^{-10} s)[53] allowing Ca^{2+} to more easily complex the anionic phosphate groups. In the systems loaded with monovalent cations in which charge shielding might be more prevalent (Fig. 4), systems loaded with larger diameter cations (e.g., K^{+}) lead to less packing compared to systems loaded with smaller diameter cations (e.g., Na^{+}).

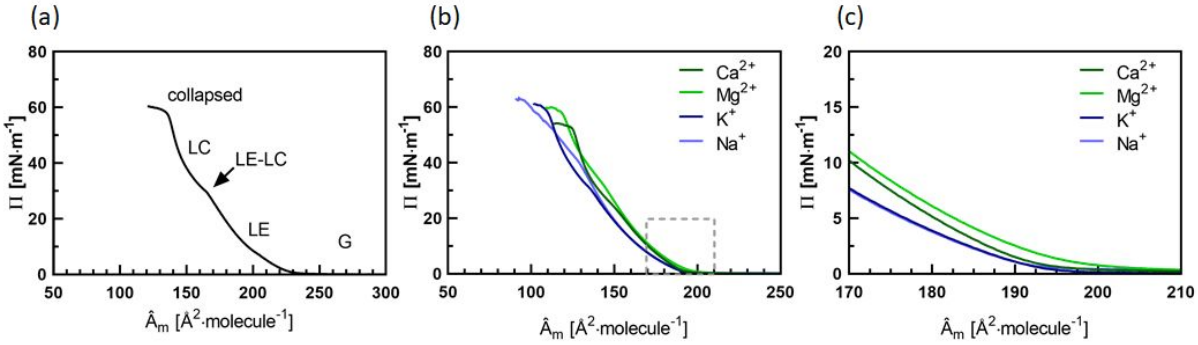

Figure 6. *Π*–$\hat{A}_m$ isotherms at 294 K for Re 595 LPS monolayers on (a) ultrapure water and (b) solutions differing in cation composition. Panel (c) shows an expanded view of the region in (b) enclosed by grey dotted rectangle. Each solution in (b) and (c) contained 3 mM equivalents of positive charge (i.e., monovalent cation concentration was 3 mM, divalent cation concentration was 1.5 mM). Metal cations were added as their chloride salts. Abbreviations: *Π*, surface pressure; $\hat{A}_m$, mean molecular area; LC, liquid condensed phase; LE, liquid expanded phase; G, bidimensional gaseous phase.

To calculate the number of bridges that ions make between carboxyl-carboxyl, carboxyl-phosphoryl or phosphoryl-phosphoryl groups, radial distances of 3 Å and 4 Å (Fig. 4) around each cation were scanned and if two carbon or phosphorous atoms (carboxyl C or phosphoryl P) are found in these regions, an ionic bridge is considered to exist. The numbers of ionic bridges obtained from this scanning method are shown in Fig. 4. These numbers represent the average values of two trajectories for each cation. This analysis shows that Ca^{2+}, despite its larger ionic radius (in comparison to Mg^{2+}), makes more ionic bridges between LPS anionic groups that leads to more LPS packing in Ca^{2+}-loaded systems. This observation is also in accord with the experimental reports that Ca^{2+}-loaded LPS bilayers experience fewer water molecule penetrations compared to Mg^{2+}- or Na^{+}-loaded LPS bilayers and there is little difference between the Mg^{2+} and Na^{+} loaded LPS bilayers implying that these two counterions have more similar effects on LPS bilayer, despite their different valence number.[28]

3.2. Intercalation of LPS with OAH

Our previous assessment of the interaction of gold nanoparticles functionalized with PAH with cell envelopes from diverse Gram-negative bacteria showed that for some bacteria the toxicity of the PAH-AuNPs is explained by the free PAH present in the suspension.[6] To probe the interactions of the 10mer oligo(allylamine HCl) surrogate for PAH equilibrated with deep rough LPS model from *S. enterica*, free energy calculations utilizing the ABF method were performed. The free energy changes were calculated while the *Z* direction distance, normal to the membrane plane (Fig. 5) between the center of mass of OAH and the center of mass of the carbon atoms of the acyl chain terminal methyl group of the lipid A sections of the LPS molecules are changed between 50 and 10 Å. To achieve more accurate results and increase the sampling at different locations, the ABF free energy calculations are performed in 10Å interval windows in the Z direction. Each window is defined by a minimum and maximum *Z* direction distance from the center of mass of the carbon atoms of the acyl chain terminal methyl group of the lipid A sections.

The free energy calculations are performed while the total volume of the systems is conserved in an NVT ensemble (constant number of atoms, volume and temperature). The change in Helmholtz free energy obtained while the OAH molecule is moved towards the hydrophobic lipid A section are shown in Fig. 5. These free energy calculations are performed for deep rough *S. enterica* LPS models after equilibration in Ca^{2+}, Mg^{2+}, Na^{+} and K^{+} ionic environments. The free energy plot indicates that divalent counterions introduce higher energy barriers against ligand than monovalent cations which highlights the importance of ion bridging and steric barriers rather than charge shielding in introducing a barrier against ligand intercalation. These differences start to become pronounced at locations that the anionic groups of the LPS arrays are present. Zero on the *x*-axis corresponds to the average surface of the LPS array and the LPS anionic groups *z*-direction distance from the average surface fall in the 0 to -10 region (highlighted by the red rectangle in Fig. 5). The minimum free energy values generally occur when the center of the mass of OAH is around 0 Å away from the average surface of the LPS core section (cf. Fig. S5 in the SI).

3.3. Surface pressure – mean molecular area isotherms for Re 595 LPS monolayers

To define the Ca^{2+} and Mg^{2+} concentrations in the solutions used to obtain surface pressure – mean molecular area (Π-$\hat{A}_m$) isotherms, we measured these elements the in water, LPS samples, and salt by ICP-MS to determine the amounts present in the subphases. The LPS solutions contain about 18 nM Ca^{2+} and 17 nM of Mg^{2+}, which corresponds to LPS-to-cation molar ratios of 556:1 and 588:1 for Ca^{2+} and Mg^{2+}, respectively. The Na^{+}- and K^{+}-containing solutions representing the subphases contained very small concentrations of Ca^{2+} and Mg^{2+} contaminants: 52 ± 2.2 nM Ca^{2+} and 22 ± 1.2 nM of Mg^{2+}. These concentrations were less than 0.0000067% and 0.0000033% of 3 mM monovalent cation solutions, respectively. The Ca^{2+}- and Mg^{2+}-containing solutions contained insignificant amount of Mg^{2+}- and Ca^{2+}- contaminants, respectively: 270 ± 81 nM Mg^{2+} (0.019% of the Ca^{2+} concentration) and 1200 ± 130 nM Ca^{2+} (0.12% of Mg^{2+} concentration), respectively. Since the level of Ca^{2+} and Mg^{2+} contamination level was quite low, we expect that the effects of contaminant Ca^{2+} and Mg^{2+} were negligible.

Figure 6 (a) shows a Π–$\hat{A}_m$ isotherm for a Re 595 LPS monolayer at the air-water interface in the absence of added salt at 294 K. The isotherm exhibits five distinct phases, each defined by calculated K_A values.[54] As surface pressure increases from 0 $mN \cdot m^{-1}$, Langmuir monolayers pass through a series of states with characteristic intermolecular interactions among molecules.[55] In the bidimensional gaseous (G) state, individual LPS molecules were well separated and conformationally disordered at the interface. Changes in surface pressure cannot be detected when the LPS molecules were in the G state.

In the absence of added ions, when the monolayer was laterally compressed such that $\hat{A}_m$ was smaller than ~232 $Å^2$, Π began to rise as LPS molecules began to interact and orient in the liquid expanded phase. As $\hat{A}_m$ decreased below ~186 $Å^2$, the monolayer transitioned to a LC phase in which the molecules were tightly packed. The transition to a plateau value at ~141 $Å^2$ signaled collapse of the monolayer, which corresponds to folding of monolayers into the subphase.[55]

We further analyzed the region of the Π–$\hat{A}_m$ isotherms where the LPS monolayer was in the LE state close to the G-to-LE phase transition to assess whether the $\hat{A}_m$ values obtained after spontaneous shrinkage in the MD simulations are plausible. We observed that the simulated LPS layers shrank after removing the restraints for equilibrium (Fig. 2B). This situation would correspond to a surface pressure somewhat higher than the transition from the G to the LE state, at which point intermolecular interactions among monolayer molecules become important. Fig. 6 (b) shows Π–$\hat{A}_m$ isotherms of LPS monolayers formed at the air–solution interface for subphases containing the indicated cations at 294 K. We calculated mean molecular areas at three monolayer compression moduli K_A using Eq. 1 relevant for the LE state (SI Table S3): 10 mN·m^{-1} to define the G-to-LE transition, 20 mN·m^{-1} as the compression modulus at which we made comparisons with simulated values of $\hat{A}_m$, and 50 mN·m^{-1} corresponding to the transition from the LE to the liquid condensed (LC) state.[44] "Tensionless" fluid lipid bilayers correspond to the LE state of lipid monolayers at the air–water interface.[56] In Table 1, each $\hat{A}_m$ value corresponds to the LE state near the G-to-LE transition defined as a K_A value exceeding 20 mN·m^{-1}. The rank order of $\hat{A}_m$ for the cations at the G-to-LE transition agrees with that determined in the simulations and the values are in good agreement (Fig. 3).

Table 1. Mean molecular areas ($\hat{A}_m$) for Re LPS molecules in the liquid expanded (LE) state near the transition from the gaseous to LE states.[a]

Cation[b]	Concentration (mM)	$\hat{A}_m$ [Å^2·molecule^{-1}]
Na^+	3	190 ± 1.0
Ca^{2+}	1.5	190 ± 3.4
K^+	3	195 ± 2.5
Mg^{2+}	1.5	198 ± 1.3

[a] K_A value exceeds 20 mN·m^{-1}. For each cation, means and standard deviations from four replicate experiments are reported.
[b] Cations added as their chloride salts.

Consistent with expectations, the isotherm of LPS monolayer on the $CaCl_2$-containing sub-phase had smaller $\hat{A}_m$ than that on $MgCl_2$-containing sub-phase, reflecting tighter packing in the presence of Ca^{2+}. Previous studies have demonstrated that divalent cations form salt bridges between among adjacent LPS molecules and increase the integrity of bacterial membrane against cationic antimicrobial peptides *in vivo*, with Ca^{2+} having a stronger effect that Mg^{2+}.[34] We found that the packing of LPS molecules in the presence of Mg^{2+} ions was not as tight as in the presence of $CaCl_2$. This result is consistent with Ca^{2+} stabilizing of LPS layers more effectively than Mg^{2+} does.

Contrary to divalent ions, overall LPS packing tendency on monovalent cation solutions was solely governed by the ionic radii. At low Π, ($\Pi \leq$ ~10 mN·m^{-1}), $\hat{A}_m$ obtained with monovalent ions were proportional to their ionic radii. This proposed that monovalent ions might produce nonspecific charge screening of LPS molecules without salt bridging as reported by Jeworrek et al.[57] We summarize our $\hat{A}_m$ values for Re LPS and selected values from the literature on various rough and wild type LPS in SI Table S4. Direct comparison of mean molecular areas among studies is complicated by differences in the purity of the LPS and salts, salt concentrations, and temperature.

4. Conclusions

In this work, we have characterized the role of metal cations in effectively controlling the insertion of a molecule —that is, OAH— into a biological surfaces in real aqueous environments. A combined use of simulation and experiment provides complementary views of the aggregation of LPS on the outer layer of the membrane. All-atom MD simulations of the equilibrations of deep rough LPS models of *Salmonella enterica* in the presence of different cations have been performed. The data presented here reveals the importance of the ionic environment on the structure and aggregation of LPS in the outer membrane of Gram-negative bacteria, and this should consequently affect their response to bactericidal agents. Specifically, we found that the aggregation was sensitive to both the degree of valency and the nature of the cation. This result is supported by measurements of effective surface area per LPS, $\hat{A}_m$, in MD simulations and in Langmuir film balance experiments. We found that a combination of ion radius and valency strongly influence the degree of LPS packing. This combined effect caused observation of increased packing with increase in the ionic radius for the LPS arrays loaded with divalent cations and decreased packing with increase in the ionic radius for the LPS arrays loaded with monovalent cations.

The initial simulations using the standard CHARMM36 force field overestimated the binding of Na^+ and K^+ to LPS molecules in comparison to the experiment. This led us to the introduction of the NBFIX correction to the CHARMM36 force field as this correction is known to resolve artifacts of interactions between monovalent cations and oxygen atoms of carboxyl and phosphoryl groups in highly charged LPS arrays. Simulations using the NBFIX feature, in which the van der Waals parameters in the CHARMM36 force field are tuned according to known benchmarks and resolving the overbinding of some monovalent cations to the LPS anionic groups, led to good agreement with experiment.

We found that cations can form bridges between carboxyl-carboxyl, carboxyl-phosphoryl and phosphoryl-phosphoryl groups in neighboring LPS molecules in bilayers. This effect seems to be more pronounced fo rLPS bilayers loaded with Ca^{2+} cation. Meanwhile, calculations of the free energy for free ligands of oligo(allylamine HCl) to intercalate into arrays of deep rough LPS of

Salmonella enterica models suggests that the strength or stability of ion bridging between LPS molecules acts against OAH intercalation. LPS arrays loaded with divalent cations exhibit larger energy barriers against intercalation of OAH. Thus stable ion bridging and steric barriers which are prevalent effects in divalent cation loaded LPS arrays rather than charge shielding which is the prevalent effect in monovalent cation loaded LPS array scan be the primary cause of the resistance to the intercalation of free ligands.

Conflicts of interest

The authors declare no competing financial interest.

Supplemental Information

Supplemental information is available online: Table S1 lists the numerical details of the quantities and size of the LPS bilayer in the model system. Table S2 provides details on the parameters used for the ICP_MS measurements. Table S3 lists the measured mean molecular areas experimentally under varying compression conditions. Table S4 compares the mean molecular areas found here to previous reports in related systems. As noted in the text, Figures S1-S5 provide visual representations of selected configurations seen in the simulations and ABF computations that illustrate the conclusions from the averaged data presented here.

Acknowledgements

This work was supported by National Science Foundation under the Center for Sustainable Nanotechnology (CSN), CHE-1503408. The CSN is part of the Centers for Chemical Innovation Program. Computing resources were provided in part by the National Science Foundation through XSEDE resources under grant number CTS090079 and by the Maryland Advanced Research Computing Center. We thank Nasim Ganji for reviewing an earlier version of this manuscript.

References

1. Beglov, D.; Roux, B. Finite representation of an infinite bulk system: Solvent boundary potential for computer simulations. *J. Chem. Phys.* **1994,** *100*, 9050-9063.
2. Huang, J.; MacKerell Jr, A. D. CHARMM36 all-atom additive protein force field: Validation based on comparison to NMR data. *J. Comput. Chem.* **2013,** *34*, 2135-2145.
3. Huang, J.; Rauscher, S.; Nawrocki, G.; Ran, T.; Feig, M.; de Groot, B. L.; Grubmüller, H.; MacKerell Jr, A. D. CHARMM36m: an improved force field for folded and intrinsically disordered proteins. *Nat. Methods.* **2016,** *14*, 71.
4. Nikaido, H.; Vaara, M. Molecular basis of bacterial outer membrane permeability. *Microbiol. Rev.* **1985,** *49*, 1.
5. Jacobson, K. H.; Gunsolus, I. L.; Kuech, T. R.; Troiano, J. M.; Melby, E. S.; Lohse, S. E.; Hu, D.; Chrisler, W. B.; Murphy, C. J.; Orr, G., et al. Lipopolysaccharide Density and Structure Govern the Extent and Distance of Nanoparticle Interaction with Actual and Model Bacterial Outer Membranes. *Environ. Sci. Technol.* **2015,** *49*, 10642-10650.

6. Buchman, J. T.; Rahnamoun, A.; Landy, K. M.; Zhang, X.; Vartanian, A. M.; Jacob, L. M.; Murphy, C. J.; Hernandez, R.; Haynes, C. L. Using an environmentally-relevant panel of Gram-negative bacteria to assess the toxicity of polyallylamine hydrochloride-wrapped gold nanoparticles. *Environ. Sci. Nano.* **2018,** *5*, 279-288.
7. Datta, A.; Ghosh, A.; Airoldi, C.; Sperandeo, P.; Mroue, K. H.; Jiménez-Barbero, J.; Kundu, P.; Ramamoorthy, A.; Bhunia, A. Antimicrobial Peptides: Insights into Membrane Permeabilization, Lipopolysaccharide Fragmentation and Application in Plant Disease Control. *Sci. Rep.* **2015,** *5*, 11951.
8. Delcour, A. H. Outer Membrane Permeability and Antibiotic Resistance. *Biochim. Biophys. Acta.* **2009,** *1794*, 808-816.
9. García-Quintanilla, M.; Pulido, M. R.; Moreno-Martínez, P.; Martín-Peña, R.; López-Rojas, R.; Pachón, J.; McConnell, M. J. Activity of Host Antimicrobials against Multidrug-Resistant *Acinetobacter baumannii* Acquiring Colistin Resistance through Loss of Lipopolysaccharide. *Antimicrob. Agents. Chemother.* **2014,** *58*, 2972-2975.
10. Grabowicz, M.; Andres, D.; Lebar, M. D.; Malojčić, G.; Kahne, D.; Silhavy, T. J. A mutant Escherichia coli that attaches peptidoglycan to lipopolysaccharide and displays cell wall on its surface. *eLife* **2014,** *3*, e05334.
11. Grossman, N.; Schmetz, M. A.; Foulds, J.; Klima, E. N.; Jimenez-Lucho, V. E.; Leive, L. L.; Joiner, K. A.; Jiminez, V. Lipopolysaccharide size and distribution determine serum resistance in Salmonella montevideo. *J. Bacteriol.* **1987,** *169*, 856-863.
12. Herrera, C. M.; Henderson, J. C.; Crofts, A. A.; Trent, M. S. Novel coordination of lipopolysaccharide modifications in Vibrio cholerae promotes CAMP resistance. *Mol. Microbiol.* **2017,** *106*, 582-596.
13. Loutet, S. A.; Flannagan, R. S.; Kooi, C.; Sokol, P. A.; Valvano, M. A. A Complete Lipopolysaccharide Inner Core Oligosaccharide Is Required for Resistance of Burkholderia cenocepacia to Antimicrobial Peptides and Bacterial Survival In Vivo. *J. Bacteriol.* **2006,** *188*, 2073-2080.
14. Maldonado, R. F.; Sá-Correia, I.; Valvano, M. A. Lipopolysaccharide modification in Gram-negative bacteria during chronic infection. *FEMS. Microbiol. Rev.* **2016,** *40*, 480-493.
15. Martinić, M.; Hoare, A.; Contreras, I.; Álvarez, S. A. Contribution of the Lipopolysaccharide to Resistance of Shigella flexneri 2a to Extreme Acidity. *PLoS. One.* **2011,** *6*, e25557.
16. Rosenfeld, Y.; Shai, Y. Lipopolysaccharide (Endotoxin)-host defense antibacterial peptides interactions: Role in bacterial resistance and prevention of sepsis. *Biochim. Biophys. Acta.* **2006,** *1758*, 1513-1522.
17. Simkovsky, R.; Effner, E. E.; Iglesias-Sánchez, M. J.; Golden, S. S. Mutations in novel lipopolysaccharide biogenesis genes confer resistance to amoebal grazing in Synechococcus elongatus. *Appl. Environ. Microbiol.* **2016,** *82*, 2738-50.
18. Tamaki, S.; Sato, T.; Matsuhashi, M. Role of Lipopolysaccharides in Antibiotic Resistance and Bacteriophage Adsorption of Escherichia coli K-12. *J. Bacteriol.* **1971,** *105*, 968-975.
19. Abadeer, N. S.; Fülöp, G.; Chen, S.; Käll, M.; Murphy, C. J. Interactions of Bacterial Lipopolysaccharides with Gold Nanorod Surfaces Investigated by Refractometric Sensing. *ACS Appl. Mater. Interfaces* **2015,** *7*, 24915-24925.
20. Vaara, M. Agents that increase the permeability of the outer membrane. *Microbiol. Rev.* **1992,** *56*, 395-411.

21. Bozich, J. S.; Lohse, S. E.; Torelli, M. D.; Murphy, C. J.; Hamers, R. J.; Klaper, R. D. Surface chemistry, charge and ligand type impact the toxicity of gold nanoparticles to *Daphnia magna*. *Environ. Sci.: Nano.* **2014,** *1*, 260-270.
22. Goodman, C. M.; McCusker, C. D.; Yilmaz, T.; Rotello, V. M. Toxicity of Gold Nanoparticles Functionalized with Cationic and Anionic Side Chains. *Bioconjug. Chem.* **2004,** *15*, 897-900.
23. Schneck, E.; Papp-Szabo, E.; Quinn, B. E.; Konovalov, O. V.; Beveridge, T. J.; Pink, D. A.; Tanaka, M. Calcium ions induce collapse of charged O-side chains of lipopolysaccharides from Pseudomonas aeruginosa. *J. R. Soc. Interface.* **2009,** *6*, S671-S678.
24. Le Brun, A. P.; Clifton, L. A.; Halbert, C. E.; Lin, B.; Meron, M.; Holden, P. J.; Lakey, J. H.; Holt, S. A. Structural Characterization of a Model Gram-Negative Bacterial Surface Using Lipopolysaccharides from Rough Strains of Escherichia coli. *Biomacromolecules* **2013,** *14*, 2014-2022.
25. Garidel, P.; Rappolt, M.; Schromm, A. B.; Howe, J.; Lohner, K.; Andrä, J.; Koch, M. H. J.; Brandenburg, K. Divalent cations affect chain mobility and aggregate structure of lipopolysaccharide from Salmonella minnesota reflected in a decrease of its biological activity. *Biochim. Biophys. Acta.* **2005,** *1715*, 122-131.
26. Clifton, L. A.; Skoda, M. W. A.; Le Brun, A. P.; Ciesielski, F.; Kuzmenko, I.; Holt, S. A.; Lakey, J. H. Effect of Divalent Cation Removal on the Structure of Gram-Negative Bacterial Outer Membrane Models. *Langmuir* **2015,** *31*, 404-412.
27. Schneck, E.; Schubert, T.; Konovalov, O. V.; Quinn, B. E.; Gutsmann, T.; Brandenburg, K.; Oliveira, R. G.; Pink, D. A.; Tanaka, M. Quantitative determination of ion distributions in bacterial lipopolysaccharide membranes by grazing-incidence X-ray fluorescence. *Proc. Natl. Acad. Sci. USA.* **2010,** *107*, 9147-9151.
28. Kučerka, N.; Papp-Szabo, E.; Nieh, M.-P.; Harroun, T. A.; Schooling, S. R.; Pencer, J.; Nicholson, E. A.; Beveridge, T. J.; Katsaras, J. Effect of Cations on the Structure of Bilayers Formed by Lipopolysaccharides Isolated from Pseudomonas aeruginosa PAO1. *J.Phys.Chem.B.* **2008,** *112*, 8057-8062.
29. Micciulla, S.; Gerelli, Y.; Schneck, E. Structure and Conformation of Wild-Type Bacterial Lipopolysaccharide Layers at Air-Water Interfaces. *Biophys. J* **2019,** *116*, 1259-1269.
30. Rodriguez-Loureiro, I.; Latza, V. M.; Fragneto, G.; Schneck, E. Conformation of Single and Interacting Lipopolysaccharide Surfaces Bearing O-Side Chains. *Biophys. J.* **2018,** *114*, 1624-1635.
31. Ma, H.; Irudayanathan, F. J.; Jiang, W.; Nangia, S. Simulating Gram-Negative Bacterial Outer Membrane: A Coarse Grain Model. *J. Phys. Chem. B.* **2015,** *119*, 14668-14682.
32. Wu, Emilia L.; Engström, O.; Jo, S.; Stuhlsatz, D.; Yeom, Min S.; Klauda, Jeffery B.; Widmalm, G.; Im, W. Molecular Dynamics and NMR Spectroscopy Studies of E. coli Lipopolysaccharide Structure and Dynamics. *Biophys J.* **2013,** *105*, 1444-1455.
33. Lam, N. H.; Ma, Z.; Ha, B.-Y. Electrostatic modification of the lipopolysaccharide layer: competing effects of divalent cations and polycationic or polyanionic molecules. *Soft Matter.* **2014,** *10*, 7528-7544.
34. Pink, D. A.; Truelstrup Hansen, L.; Gill, T. A.; Quinn, B. E.; Jericho, M. H.; Beveridge, T. J. Divalent Calcium Ions Inhibit the Penetration of Protamine through the Polysaccharide Brush of the Outer Membrane of Gram-Negative Bacteria. *Langmuir* **2003,** *19*, 8852-8858.

35. Kim, S.; Patel, Dhilon S.; Park, S.; Slusky, J.; Klauda, Jeffery B.; Widmalm, G.; Im, W. Bilayer Properties of Lipid A from Various Gram-Negative Bacteria. *Biophys. J.* **2016,** *111*, 1750-1760.
36. Piggot, T. J.; Holdbrook, D. A.; Khalid, S. Conformational dynamics and membrane interactions of the E. coli outer membrane protein FecA: A molecular dynamics simulation study. *Biochim. Biophys. Acta.* **2013,** *1828*, 284-293.
37. Kirschner, K. N.; Lins, R. D.; Maass, A.; Soares, T. A. A Glycam-Based Force Field for Simulations of Lipopolysaccharide Membranes: Parametrization and Validation. *J. Chem. Theory. Comput.* **2012,** *8*, 4719-4731.
38. Murzyn, K.; Pasenkiewicz-Gierula, M. Structural Properties of the Water/Membrane Interface of a Bilayer Built of the E. coli Lipid A. *J Phys Chem B.* **2015,** *119*, 5846-5856.
39. Nascimento, A.; Pontes, F. J. S.; Lins, R. D.; Soares, T. A. Hydration, ionic valence and cross-linking propensities of cations determine the stability of lipopolysaccharide (LPS) membranes. *Chem. Commun. (Camb).* **2014,** *50*, 231-233.
40. Nelson, M. T.; Humphrey, W.; Gursoy, A.; Dalke, A.; Kalé, L. V.; Skeel, R. D.; Schulten, K. NAMD: a Parallel, Object-Oriented Molecular Dynamics Program. *J. Supercomputing. App.* **1996,** *10*, 251-268.
41. Comer, J.; Gumbart, J. C.; Hénin, J.; Lelièvre, T.; Pohorille, A.; Chipot, C. The Adaptive Biasing Force Method: Everything You Always Wanted To Know but Were Afraid To Ask. *J. Phys. Chem. B.* **2015,** *119*, 1129-1151.
42. Langmuir, I. The Constitution And Fundamental Properties of Solids and Liquids. II. Liquids. *J. Am. Chem. Soc.* **1917,** *39*, 1848-1906.
43. Zhang, T.; Cathcart, M. G.; Vidalis, A. S.; Allen, H. C. Cation effects on phosphatidic acid monolayers at various pH conditions. *Chem. Phys. Lipids* **2016,** *200*, 24-31.
44. Kodama, M.; Shibata, O.; Nakamura, S.; Lee, S.; Sugihara, G. A monolayer study on three binary mixed systems of dipalmitoyl phosphatidyl choline with cholesterol, cholestanol and stigmasterol. *Colloids. Surf. B.* **2004,** *33*, 211-226.
45. Ulman, A., *An introduction to ultrathin organic films : from Langmuir-Blodgett to self-assembly*. Elsevier Inc.: Boston, 1991.
46. McGuigan, J. A.; Lüthi, D.; Buri, A. Calcium buffer solutions and how to make them: a do it yourself guide. *Can. J. Physiol. Pharmacol.* **1991,** *69*, 1733.
47. Shands, J. W.; Chun, P. W. The dispersion of Gram-negative lipopolysaccharide by deoxycholate. *J Biol. Chem.* **1980,** *255*, 1221-1226.
48. Okuda, T.; Schauer, J. J.; Shafer, M. M. Improved methods for elemental analysis of atmospheric aerosols for evaluating human health impacts of aerosols in East Asia. *Atmos. Environ.* **2014,** *97*, 552.
49. Herrmann, M.; Schneck, E.; Gutsmann, T.; Brandenburg, K.; Tanaka, M. Bacterial lipopolysaccharides form physically cross-linked, two-dimensional gels in the presence of divalent cations. *Soft Matter* **2015,** *11*, 6037-6044.
50. Yoo, J.; Aksimentiev, A. Improved Parametrization of Li+, Na+, K+, and Mg2+ Ions for All-Atom Molecular Dynamics Simulations of Nucleic Acid Systems. *J. Phys. Chem. Lett.* **2012,** *3*, 45-50.
51. Venable, R. M.; Luo, Y.; Gawrisch, K.; Roux, B.; Pastor, R. W. Simulations of anionic lipid membranes: development of interaction-specific ion parameters and validation using NMR data. *J. Phys. Chem. B.* **2013,** *117*, 10183-10192.

52. Nightingale, E. R. Phenomenological Theory of Ion Solvation. Effective Radii of Hydrated Ions. *J. Phys. Chem.* **1959,** *63*, 1381-1387.
53. Lee, Y.; Thirumalai, D.; Hyeon, C. Ultrasensitivity of water exchange kinetics to the size of metal ion. *Journal of the American Chemical Society* **2017,** *139*, 12334-12337.
54. Davies, J. T., *Interfacial phenomena*. 2nd ed.; Academic Press: New York, 2012.
55. Baoukina, S.; Monticelli, L.; Risselada, H. J.; Marrink, S. J.; Tieleman, D. P. The molecular mechanism of lipid monolayer collapse. *Proc. Natl. Acad. Sci. U.S.A.* **2008,** *105*, 10803.
56. Marsh, D. Lateral pressure in membranes. *Biophys. Biochim. Acta* **1996,** *1286*, 183-223.
57. Jeworrek, C.; Evers, F.; Howe, J.; Brandenburg, K.; Tolan, M.; Winter, R. Effects of specific versus nonspecific ionic interactions on the structure and lateral organization of lipopolysaccharides. *Biophys. J.* **2011**, 2169-77.

TOC graphic

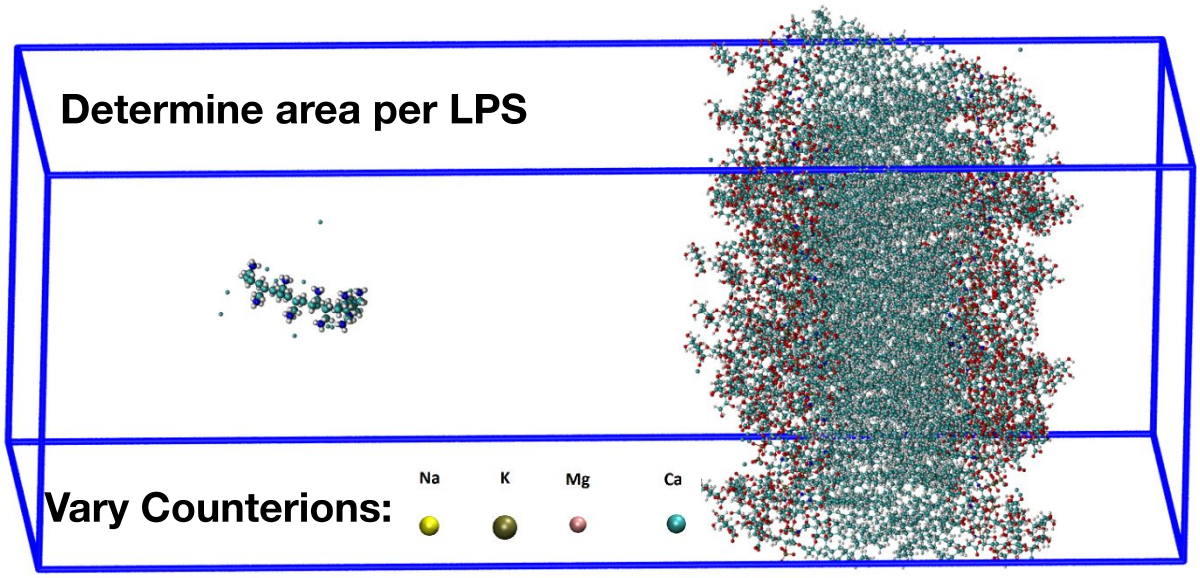

A)

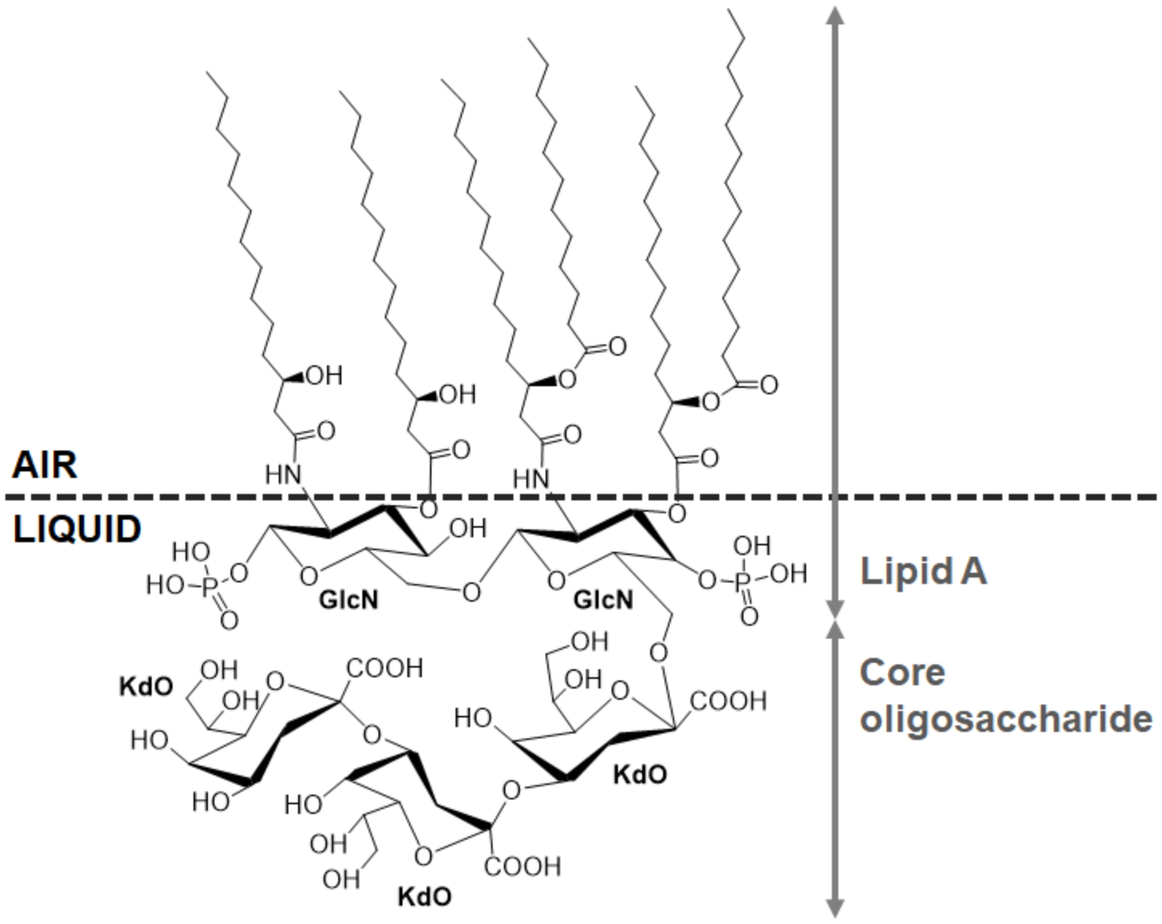
AIR
LIQUID
HN
HN
OH
HO
HO-P-O
O
GlcN
GlcN
O-P-OH
Lipid A
KdO
COOH
KdO
KdO
Core
oligosaccharide

B)

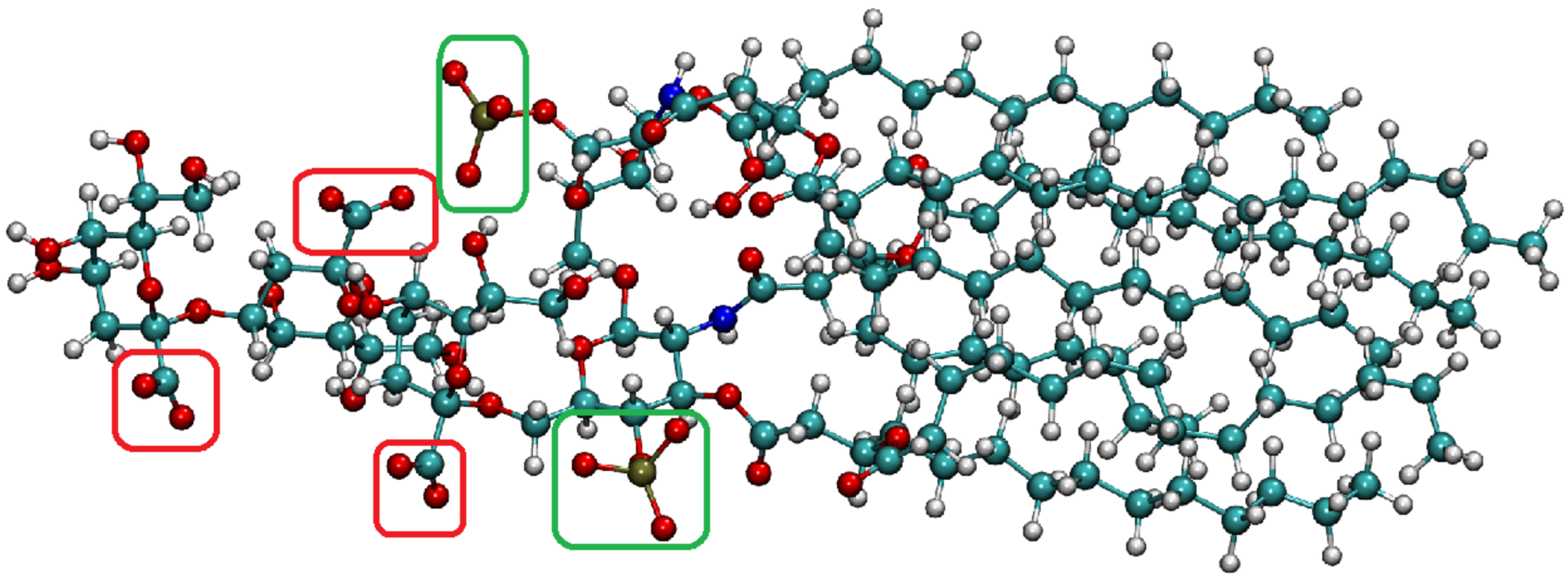

C)

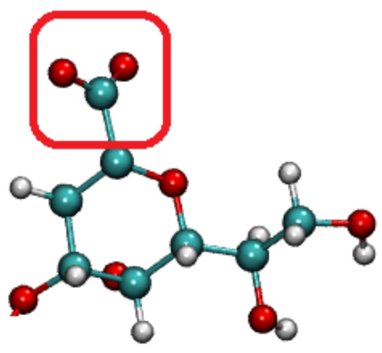

D)

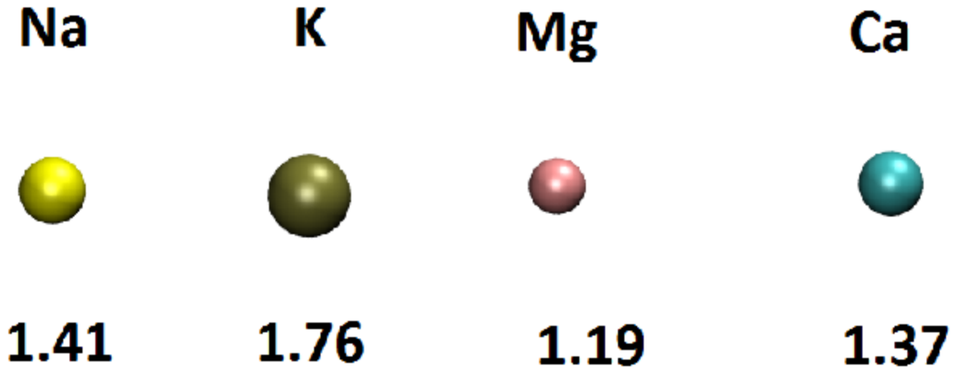
Na
K
Mg
Ca
1.41
1.76
1.19
1.37

A

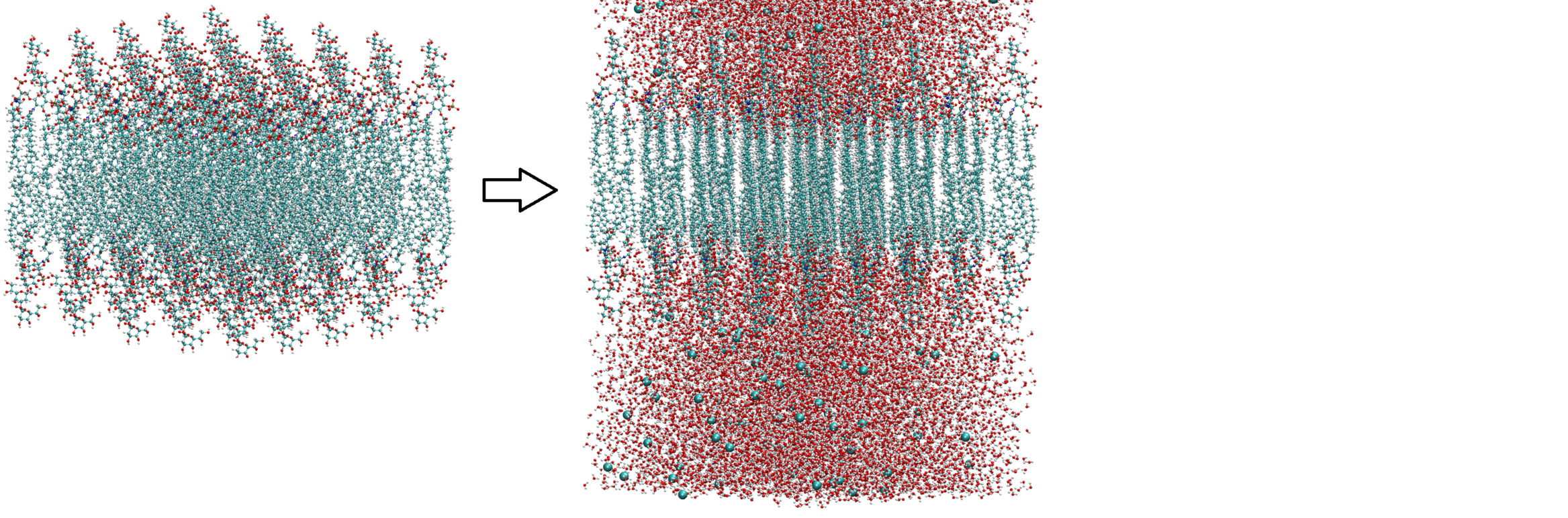

B

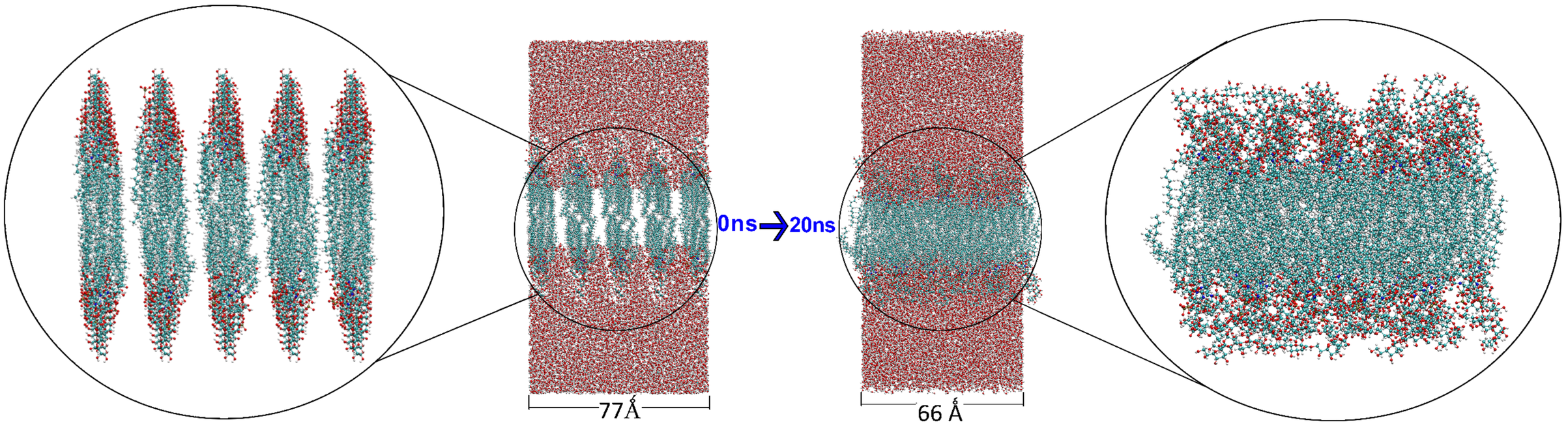

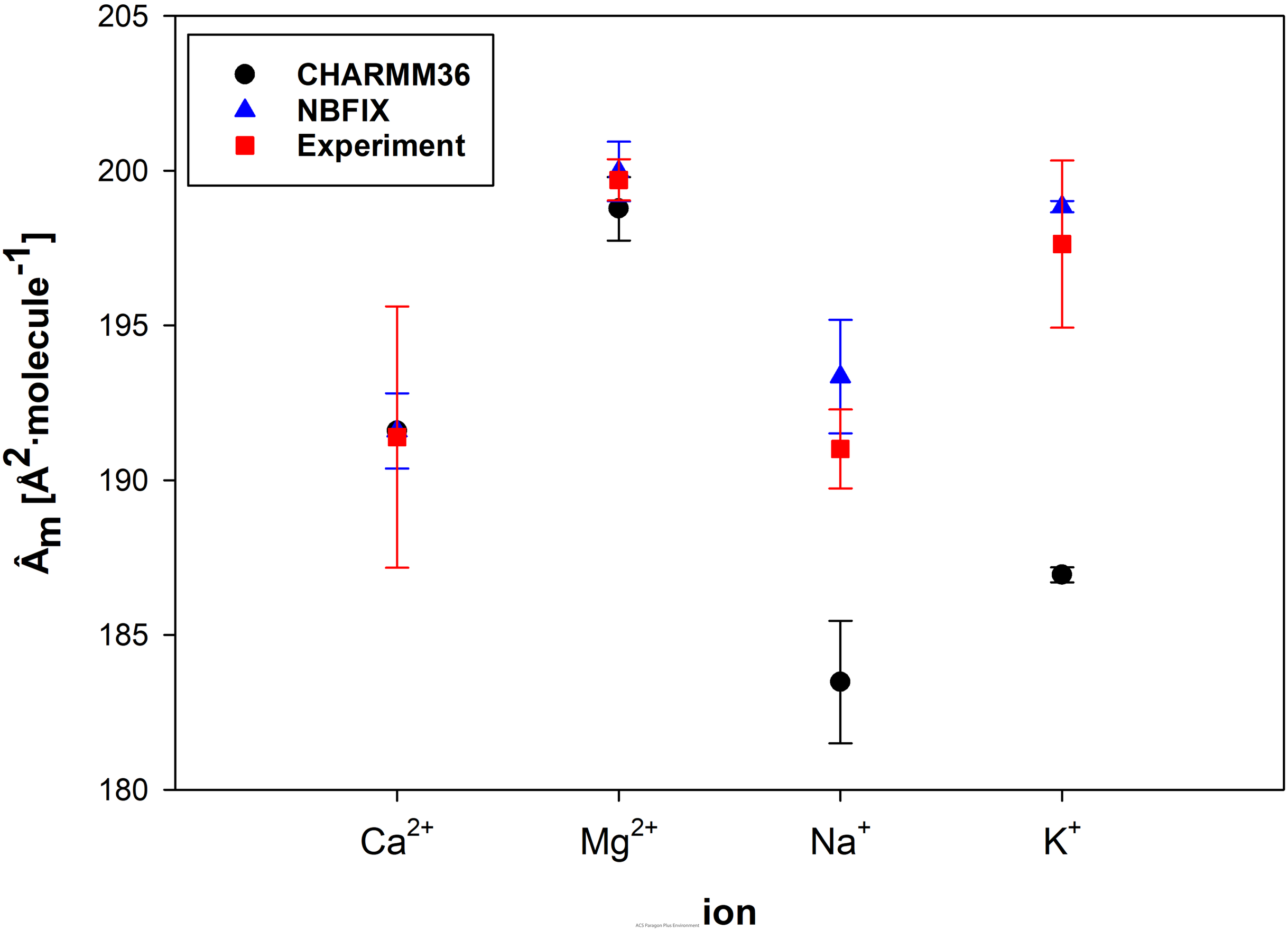
CHARMM36
NBFIX
Experiment
205
200
195
190
185
180
Âm [Å2·molecule-1]
Ca2+
Mg2+
Na+
K+
ion

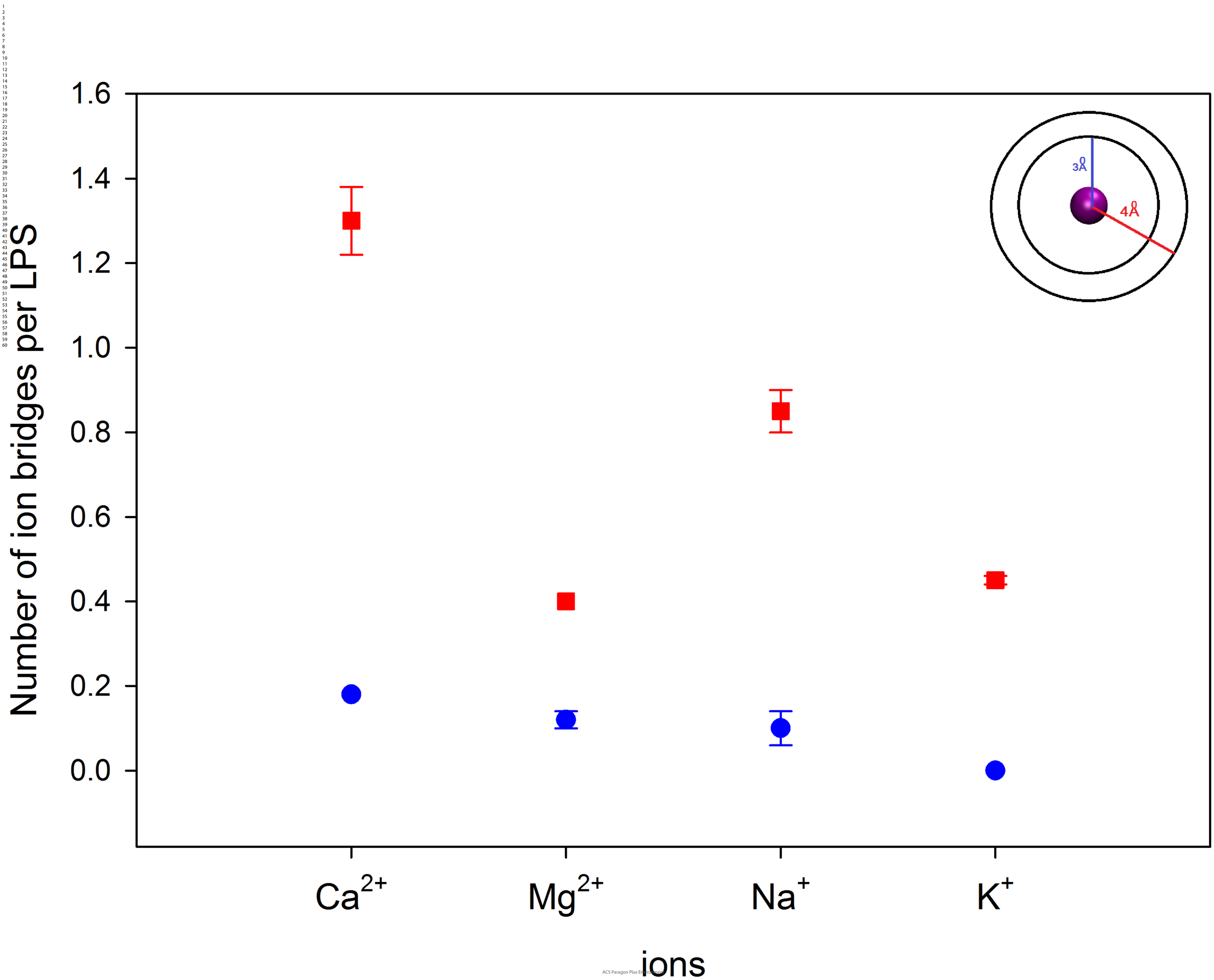
Number of ion bridges per LPS
1.6
1.4
1.2
1.0
0.8
0.6
0.4
0.2
0.0
3Å
4Å
Ca2+
Mg2+
Na+
K+
ions

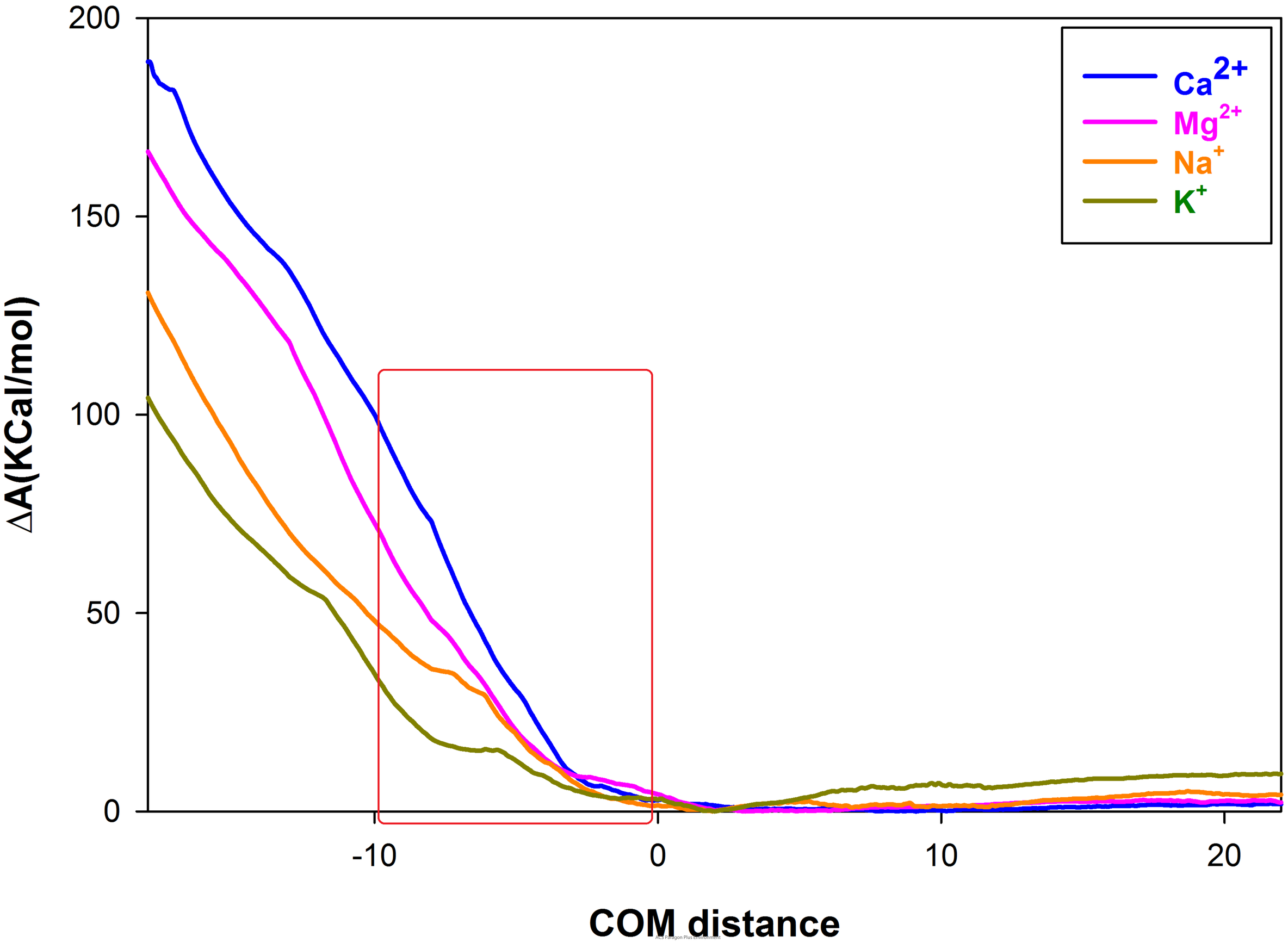
200
150
100
50
0
ΔA(KCal/mol)
-10
0
10
20
COM distance
Ca2+
Mg2+
Na+
K+

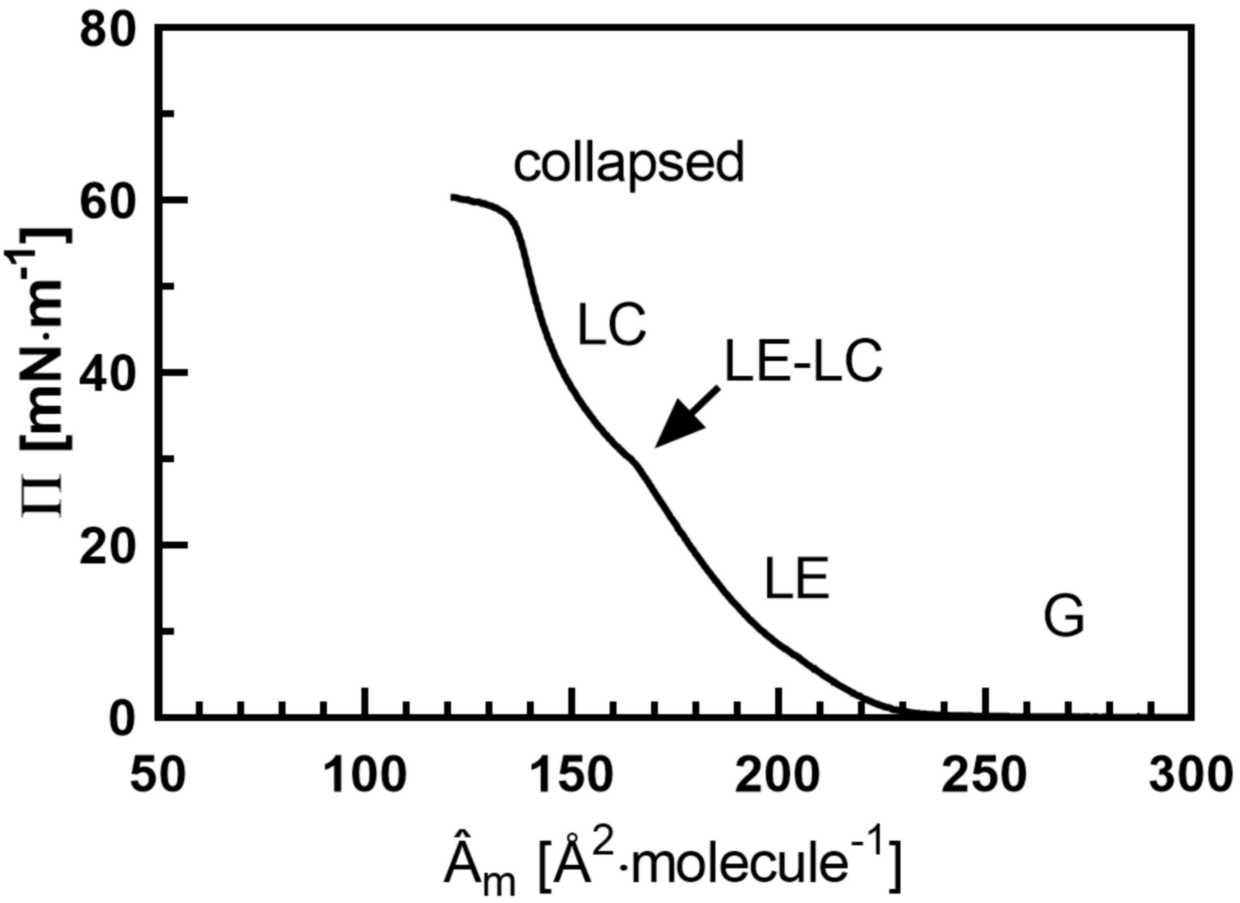
80
60
40
20
0
Π [mN·m-1]
collapsed
LC
LE-LC
LE
G
50
100
150
200
250
300
Âm [Å2·molecule-1]

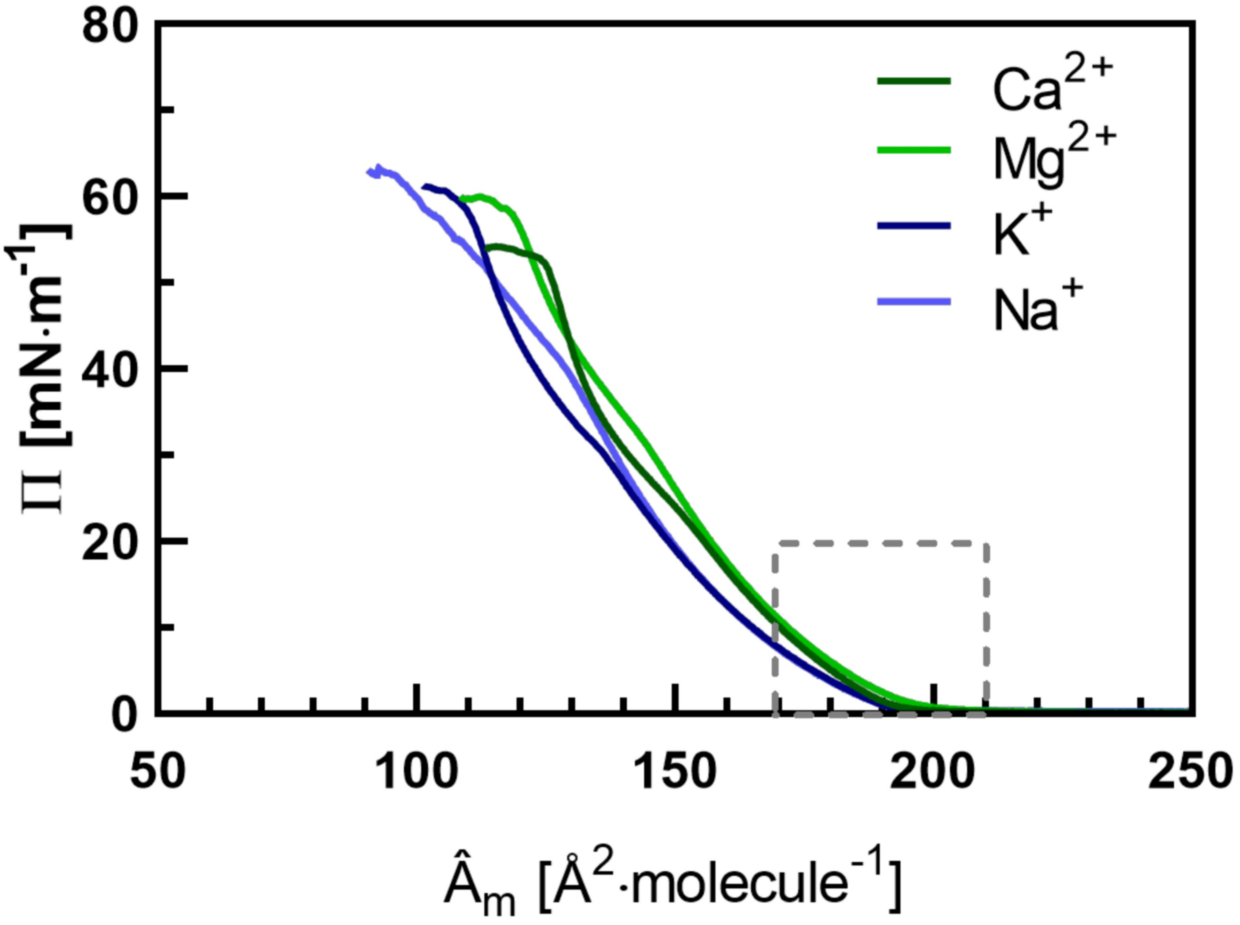
80
60
40
20
0
Π [mN·m-1]
50
100
150
200
250
Âm [Å2·molecule-1]
Ca2+
Mg2+
K+
Na+

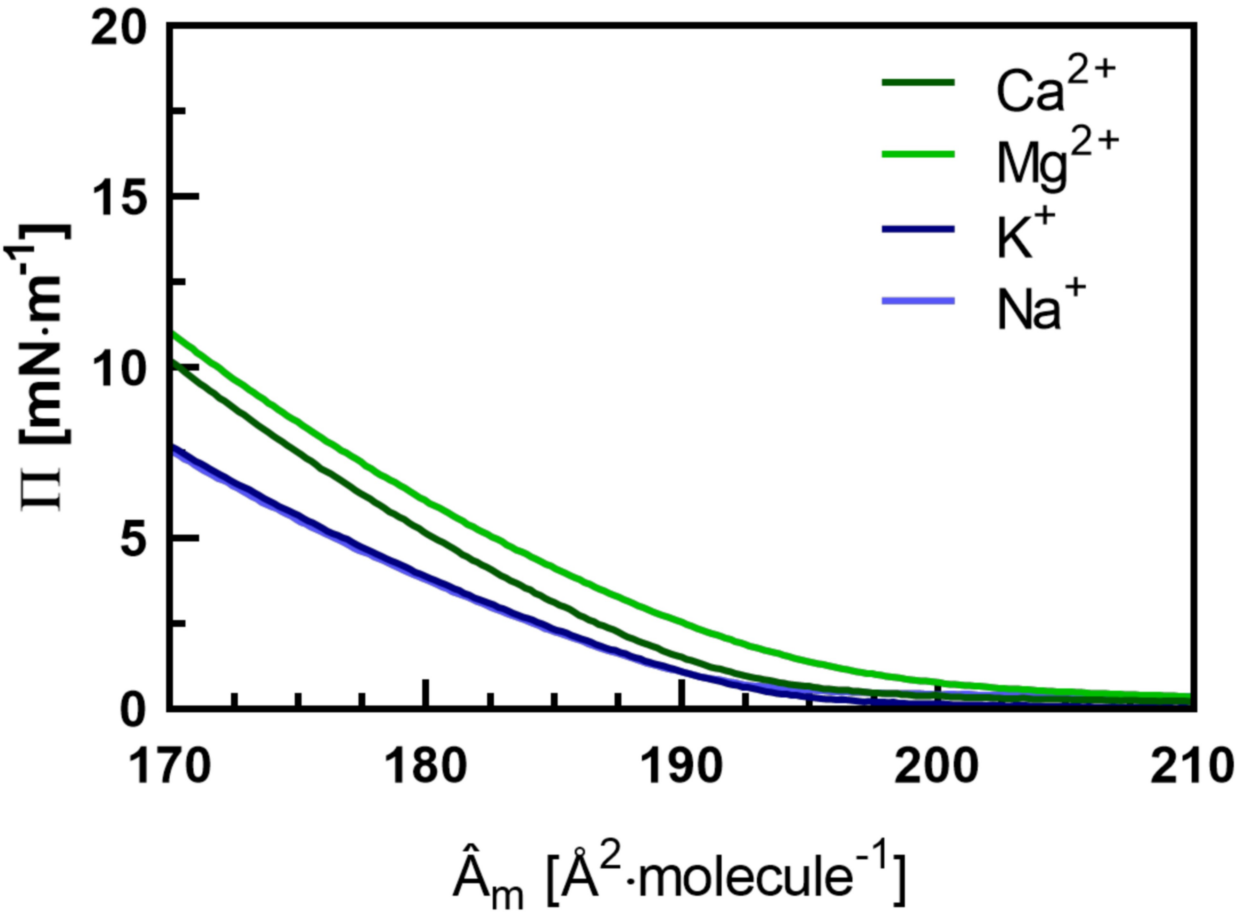
20
15
10
5
0
170
180
190
200
210
Π [mN·m-1]
Âm [Å2·molecule-1]
Ca2+
Mg2+
K+
Na+